(4)

Aerodynamic Side Force Induced
by Nozzle Entrance Flow Asymmetry

R. L. VARWIG, J. S. WHITTIER, and D. A. DURRAN
Aerophysics Laboratory
Laboratory Operations

R. X. MEYER and E. K. RUTH
Engineering Group
The Aerospace Corporation
El Segundo, CA 90245

AD-A206 631

DTIC
SELECTED
APR 1 1 1989
D

D ⊂ℰ

-1 October 1988

Prepared for

SPACE DIVISION
AIR FORCE SYSTEMS COMMAND
Los Angeles Air Force Base
P.O. Box 92960, Worldway Postal Center
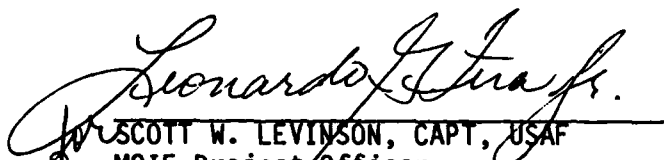Los Angeles, CA 90009-2960

BEST
AVAILABLE COPY

89 4 10 017

This report was submitted by The Aerospace Corporation, El Segundo, CA 90245, under Contract No. F04701-85-C-0086-P00019 with the Space Division, P.O. Box 92960, Los Angeles, CA 90009-2960. It was reviewed and approved for The Aerospace Corporation by W.P. Thompson, Director, Aerophysics Laboratory.

Capt Scott W. Levinson was the Air Force project officer.

This report has been reviewed by the Public Affairs Office (PAS) and is releasable to the National Technical Information Service (NTIS). At NTIS, it will be available to the general public, including foreign nationals.

This technical report has been reviewed and is approved for publication. Publication of this report does not constitute Air Force approval of the report's findings or conclusions. It is published only for the exchange and stimulation of ideas.

SCOTT W. LEVINSON, CAPT, USAF
MOIE Project Officer
SD/CNID

JAMES A. BERES, LT COL, USAF
MOIE Program Manager
AFSTC/WCO OL-AB

REPORT DOCUMENTATION PAGE

1a. REPORT SECURITY CLASSIFICATION Unclassified			1b. RESTRICTIVE MARKINGS	
2a. SECURITY CLASSIFICATION AUTHORITY			3. DISTRIBUTION/AVAILABILITY OF REPORT Approved for public release; distribution unlimited.	
2b. DECLASSIFICATION/DOWNGRADING SCHEDULE				
4. PERFORMING ORGANIZATION REPORT NUMBER(S) TR-0088(3470-02)-1			5. MONITORING ORGANIZATION REPORT NUMBER(S) SD-TR-89-12	
6a. NAME OF PERFORMING ORGANIZATION The Aerospace Corporation Laboratory Operations	6b. OFFICE SYMBOL (If applicable)		7a. NAME OF MONITORING ORGANIZATION Space Division	
6c. ADDRESS (City, State, and ZIP Code) El Segundo, CA 90245			7b. ADDRESS (City, State, and ZIP Code) Los Angeles Air Force Base Los Angeles, CA 90009-2960	
8a. NAME OF FUNDING/SPONSORING ORGANIZATION	8b. OFFICE SYMBOL (If applicable)		9. PROCUREMENT INSTRUMENT IDENTIFICATION NUMBER F04701-85-C-0086-P00019	
8c. ADDRESS (City, State, and ZIP Code)			10. SOURCE OF FUNDING NUMBERS	

PROGRAM ELEMENT NO.	PROJECT NO.	TASK NO.	WORK UNIT ACCESSION NO.

11. TITLE (Include Security Classification)
Aerodynamic Side Force Induced by Nozzle Entrance Flow Asymmetry

12. PERSONAL AUTHOR(S)
Varwig, Robert L.; Whittier, James S.; Durran, Donald A.; Meyer, Rudolf X.; Ruth, Edward K.

13a. TYPE OF REPORT	13b. TIME COVERED FROM _____ TO _____	14. DATE OF REPORT (Year, Month, Day) 1988 October 1	15. PAGE COUNT 27

16. SUPPLEMENTARY NOTATION

17. COSATI CODES			18. SUBJECT TERMS (Continue on reverse if necessary and identify by block number)
FIELD	GROUP	SUB-GROUP	

19. ABSTRACT (Continue on reverse if necessary and identify by block number)

The Star 48 upper stage rocket motor and payload system appears to precess in a coning motion which affects the flight path. The coning motion has been attributed to side forces generated because of deviations of the rocket nozzle entrance flow from truly axisymmetric conditions. In this report, an experimental investigation is described in which intentional nozzle entrance flow misalignment was produced and consequent side force was measured on a model at a simulated altitude of 1.7 x 10^5 ft. 175,0 ft.

Side forces generated with an approximately 1/50th scale Star 48 rocket nozzle were quite small when compared to the predictions and measurements of previous investigators, but the difference was attributed to the difference where the flow inclination or misalignment occurs. When the flow is inclined at the nozzle throat, the downstream effect of the inclination is predictably large. When the flow is inclined in the plenum upstream of the nozzle entrance, the downstream effect is smaller by an order of magnitude. The observed side forces show a dependence on the nozzle length, as indicated by earlier investigators.

20. DISTRIBUTION/AVAILABILITY OF ABSTRACT ☒ UNCLASSIFIED/UNLIMITED ☐ SAME AS RPT. ☐ DTIC USERS		21. ABSTRACT SECURITY CLASSIFICATION Unclassified	
22a. NAME OF RESPONSIBLE INDIVIDUAL		22b. TELEPHONE (Include Area Code)	22c. OFFICE SYMBOL

DD FORM 1473, 84 MAR
83 APR edition may be used until exhausted.
All other editions are obsolete.

SECURITY CLASSIFICATION OF THIS PAGE

UNCLASSIFIED

PREFACE

The authors wish to acknowledge the contributions of Richard Aurandt who assembled and prepared the model for testing and who was instrumental in running the tests.

Accesion For		
NTIS CRA&I	☑	
DTIC TAB	☐	
Unannounced	☐	
Justification		
By		
Distribution /		
Availability Codes		
Dist	Avail and/or Special	
A-1		

CONTENTS

FIGURES

3

I. INTRODUCTION

With spin-stabilized space vehicles, turning moments are observed that can lead to a coning motion in which the center of mass precesses about an axis through the nose of the vehicle, leading to instability and control problems. Coning occurs in the Star 48 upper stage rocket motor. Among potential causes for the turning moments are deviations of the rocket nozzle entrance flow from truly axisymmetric conditions.

Meyer (Reference 1) attributed the rocket motor gas flow deflection to the effect of Coriolis forces on the spinning vehicle. Darwell and Trubridge (Reference 2), Hoffman and Maykut (Reference 3), and Walters (Reference 4), calculated side force and moment on rocket nozzles from assumptions of angular misalignment and showed that the side force and moments varied in a damped sinusoidal manner with nozzle length. Darwell, Trubridge, and Walters also conducted experiments which verified their calculations. In these analyses, the flow is assumed to be misaligned at the throat. Hoffman and Maykut define an initial value surface which is a constant property plane at the throat pitched at an angle with respect to the axis of an axisymmetric nozzle exit contour. In the experiments of Walters, the nozzles he studied either had the throat extended on one side, or the throat entrance section shortened and tilted on one side, producing an asymmetric throat or throat entrance section in each case. Thus, a canted flow was produced at the throat as assumed in the analysis.

In the experiment that we propose, the nozzle and entrance section are assumed to be properly designed and fabricated axisymmetric components. Only the flow entering the nozzle is turned, for example, by the Coriolis forces suggested by Meyer. We therefore propose to evaluate the asymmetries associated with an axisymmetric nozzle in which the nozzle plenum flow is inclined with respect to the nozzle axis.

To do this, we built a force model in which misalignment of flow at the nozzle entrance could be produced, incorporating as much as practical the Star 48 nozzle configuration. In this way, we could observe whether the turning

moments observed in the Star 48 system were connected with flow misalignment at the nozzle entrance. Since the Star 48 flies at a high altitude, we proposed to perform the experiments in a large vacuum tank which could be pumped down to a pressure simulating 1.7×10^5 ft.

In this report, the model is described, and the side force measurements are presented for several nozzles of different lengths, expansion angles, and throat design. The observed side forces for these nozzles did depend on nozzle length, although their magnitudes were much smaller than those described in References 2, 3, and 4.

II. EXPERIMENTAL APPARATUS AND TESTS

The apparatus which was developed is shown schematically in Figures 1 and 2. It consists of a nozzle, tanks to contain the gas for the flow and a framework for supporting these components, and for providing an axis normal to the thrust direction about which the model is constrained to rotate.

The flow misalignment or asymmetry is provided by tilting the supply tube (Figure 2) for the nozzle plenum. The deflection angle is about 7.5 deg, and the tube can be rotated 180 deg so that differences of 15 deg in flow deflection can be obtained. A straight tube is also available which should supply flow nominally aligned with the nozzle axis for baseline data. A photograph of the assembled apparatus is shown in Figure 3.

The forces on the rig can be considered from the geometric model of Figure 4. Here, the force model is shown with nozzle axis aligned with the center of gravity (c.g.) of the force model and the flow misaligned by angle δ with respect to the nozzle axis. The forces on the rig include the side force, F_y, from pressure forces applied to the nozzle walls and the moment, M_z, resulting from the velocity gradient at the throat. The measured side force is a response to these combined forces. When δ is small so that the sine can be approximated by the angle in radians, the total moment about the model c.g. is given as

$$M_{cg} = F_y \ell + M_z = (\text{Meas. Force}) \times 18.0 \text{ in.}$$

The moment M_z assumes a force acting along the throat radius y_t. Eighteen inches is the distance from the rig c.g. to the point where the force is applied which is defined by the calibration process.

Three nozzles (Figures 5, 6, and 7) were built for use in this experiment. The shortest of the three is an adaption of the nozzle for the Star 48 upper stage rocket motor. The next nozzle was longer with a larger throat radius of curvature, and the last nozzle (actually three since it was cut progressively to three different lengths) was built according to the analysis
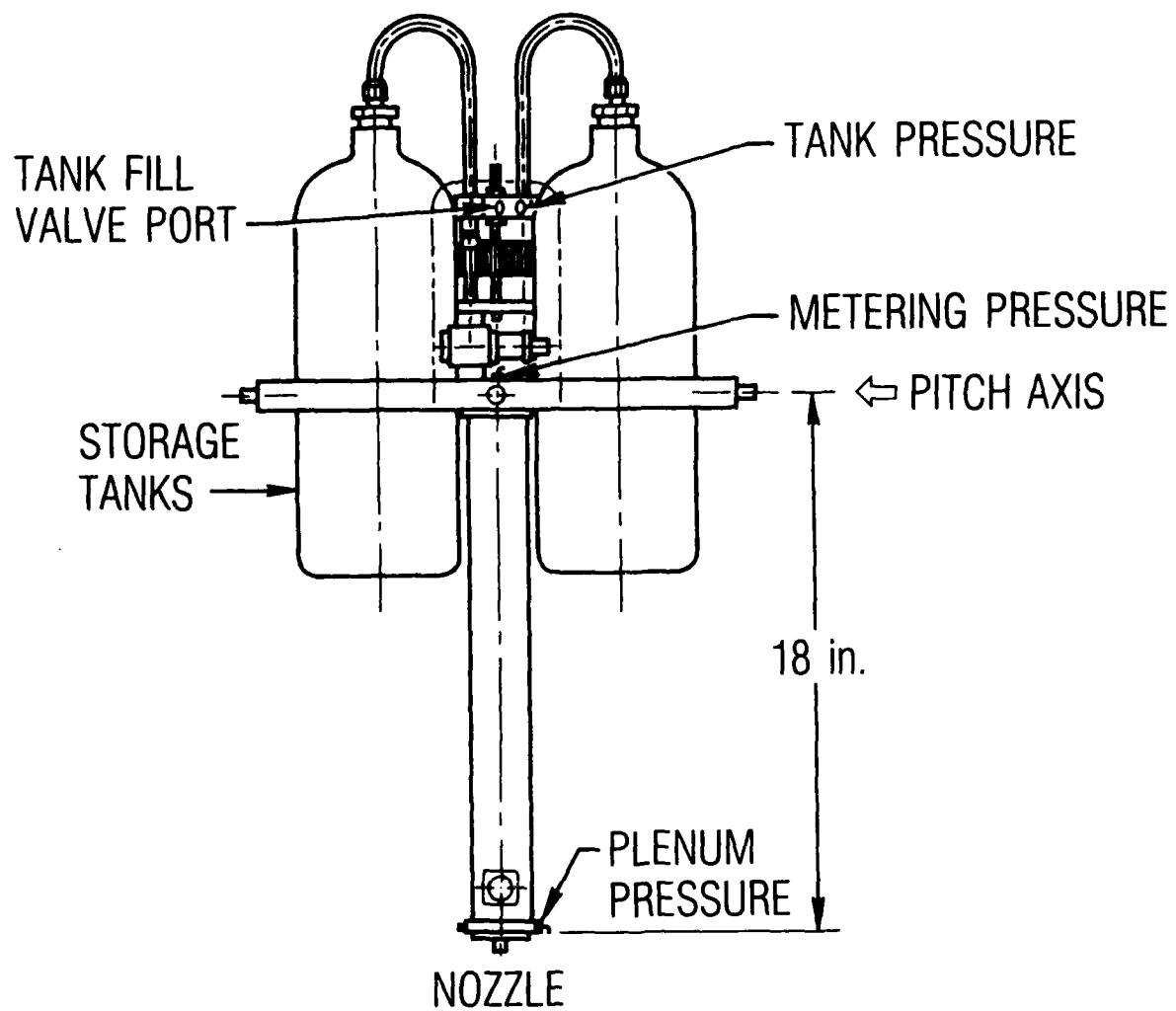
7

Figure 1. Idealized one-degree-of-freedom experimental model.

INCLINED FLOW
FILL TUBE

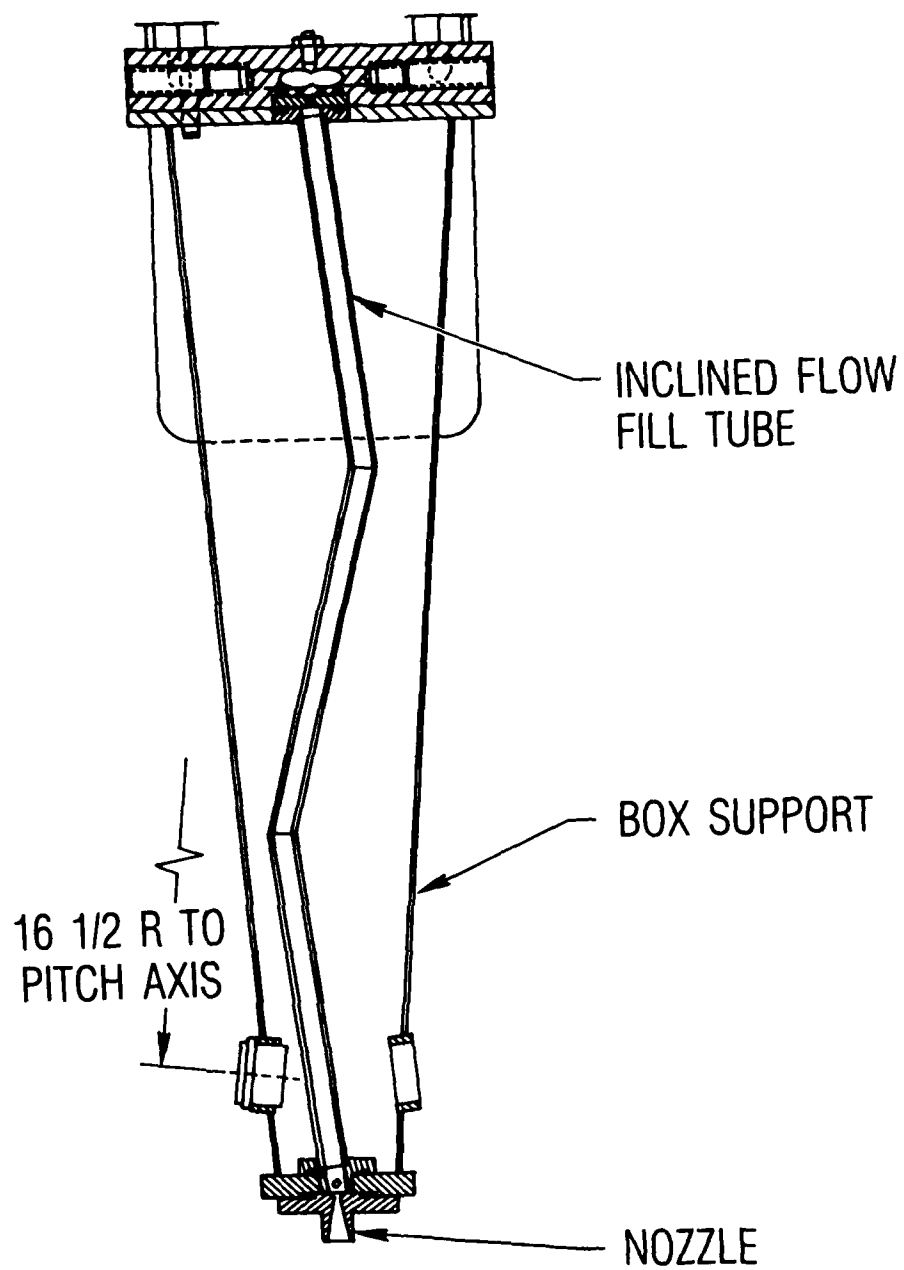BOX SUPPORT

16 1/2 R TO
PITCH AXIS

NOZZLE

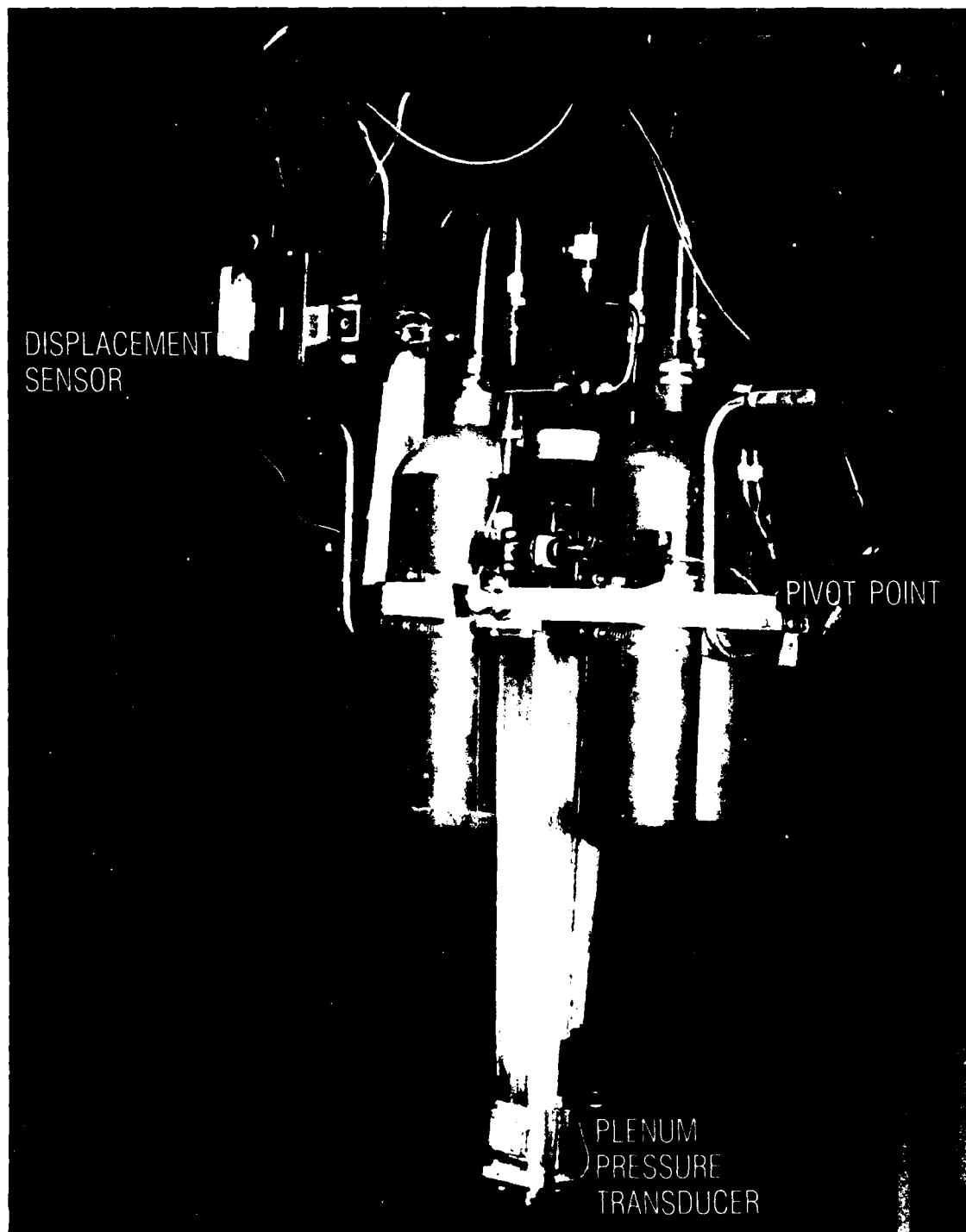Figure 2. Production of asymmetric nozzle entrance flow.

Figure 3. Side force model mounted in vacuum tank.

δ = FLOW MISALIGNMENT
    ANGLE

TOTAL MOMENT ABOUT
MODEL C.G.:

$$M_{C.G.} = F_y \ell + M_z$$
$$= \text{(measured side force) 18 in.}$$

MODEL
C.G.

18 in.

ℓ

MEASURED
SIDE FORCE

F_x

δ

F_y

M_z

NOZZLE
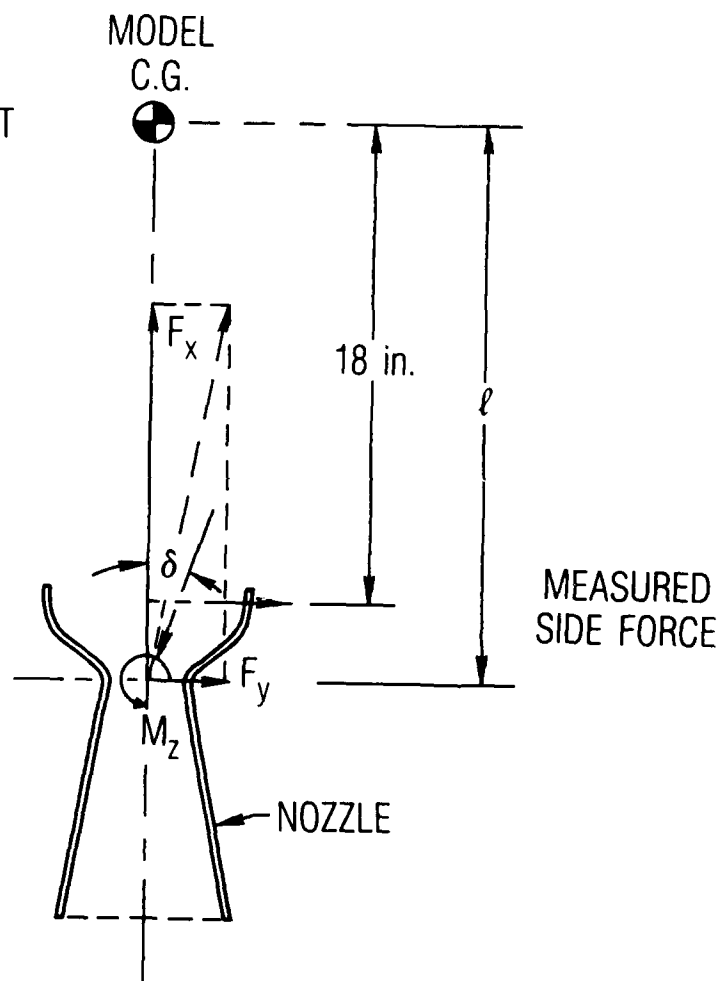
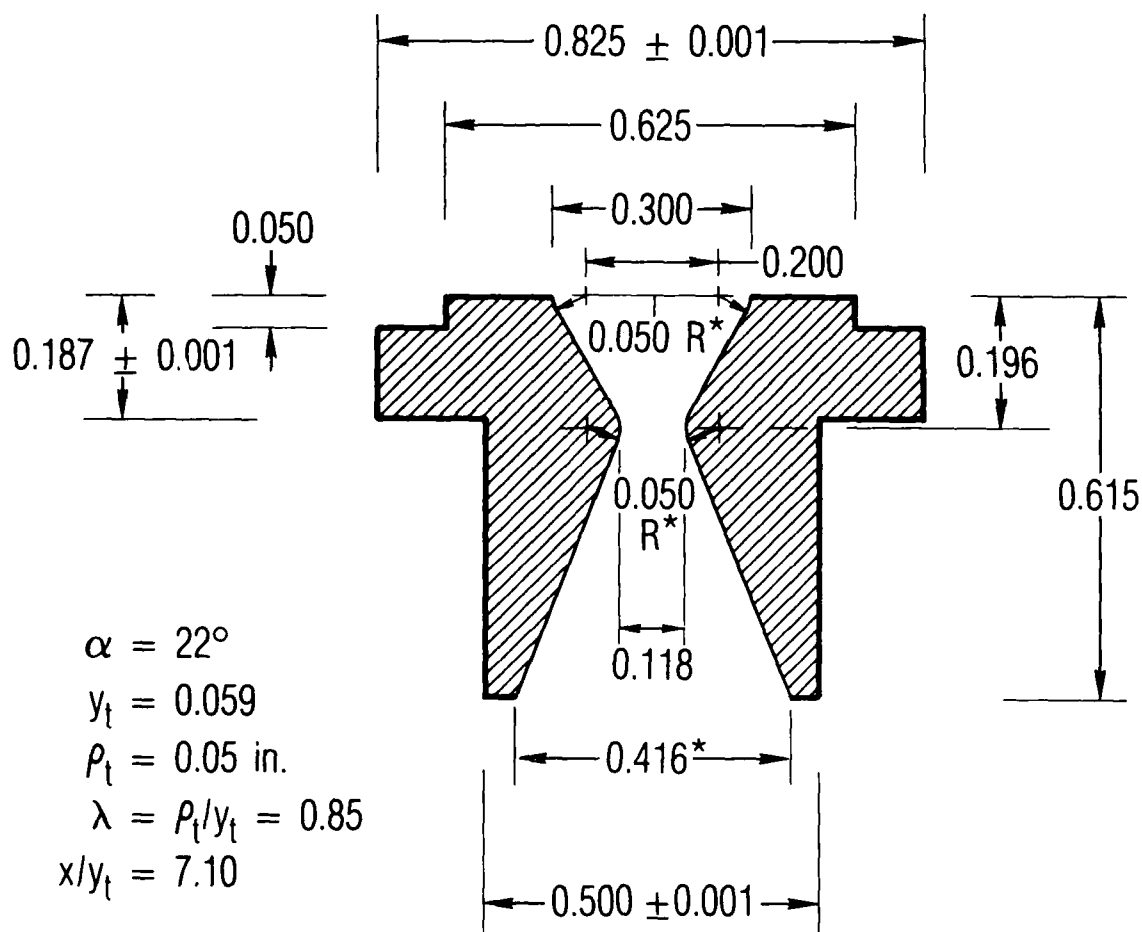Figure 4.   Forces, moments on model with misaligned entry flow.

11

Figure 5.   1/50 scale Star 48 nozzle model, nozzle number 4,
A/A* = 12.43, M = 4.17.

12
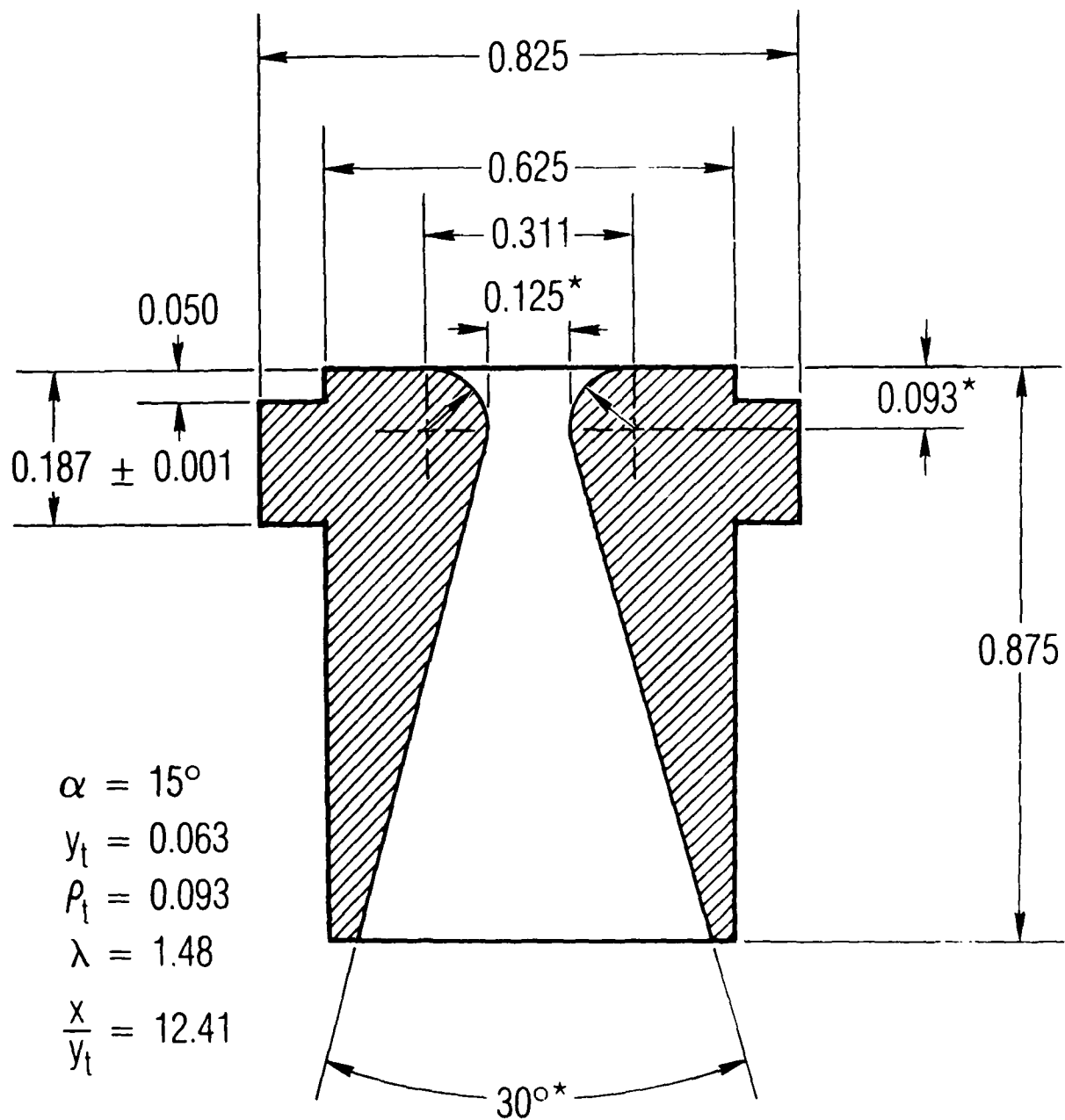
Figure 6. Nozzle number 3, A/A* = 18.66, M = 4.64.

$\alpha = 15°$

$y_t = 0.063$

$\rho_t = 0.093$

$\lambda = 1.48$

$\dfrac{x}{y_t} = 12.41$

13

Figure 7. Nozzle designed from Reference 3 analysis.

NOZZLE No. 5, 6, 7

$A/A^* = 9.61$

$\alpha = 10°$

$y_t = 0.0625$ in.

$\rho_t = 0.0312$ in.

$\lambda = 0.5$

14

of Reference 3 to correspond with the curve of Figure 3 of Reference 3 for cone half angle, α, = 10 deg.

The side force is determined from a measurement of the displacement of one end of the model as it rotates during the test. The displacement is sensed by a Schaevitz Engineering Linear Variable Differential Transformer (LVDT). Calibration is provided in terms of force by hanging weights on the model using a pulley to orient the calibrating force along the direction of the expected applied force. The load causes a static deflection of the model. To provide a dynamic calibration, the weight-supporting wire is melted by an electric current impulsively applied. Thus, an impulsive, negative load is applied and the response of the model is observed from the LVDT signal. The force is determined from an average value of the LVDT signal. A typical calibration test and subsequent force calibration are shown in Figure 8.

The plenum pressure is measured by an Endevco strain gauge transducer installed just upstream of the nozzle throat. From the plenum pressure, the thrust is calculated according to

$$\text{Thrust} = (1/2)\ (1 + \cos\alpha)\ \dot{m}\ V_e + (p_e - p_a)A_e$$

or in terms of measured values

$$= (1 + \cos\alpha)\ 0.290\ p_o\ \gamma A^* M\ \sqrt{(1 + M^2/5)^{-1}} + (p_e - p_a)A_e$$

Here, α is the nozzle cone half-angle; p_o is the measured plenum pressure, A^* and A_e are throat and nozzle exit areas; M is the exit Mach number; p_e and p_a are exit and ambient static pressures. γ is assumed to be 1.4 for nitrogen, which is the gas used in the tests. Mach number and static pressure are calculated from the exit-throat area ratio, data for which have been conveniently tabulated in years past. The ambient pressure, p_a, in these tests is so low relative to p_e, that the correction term $(p_e - p_a)A_e$ is reduced to $p_e A_e$.
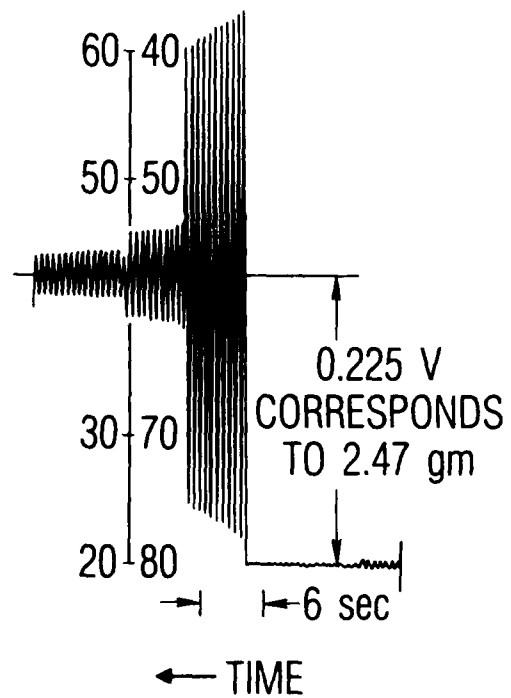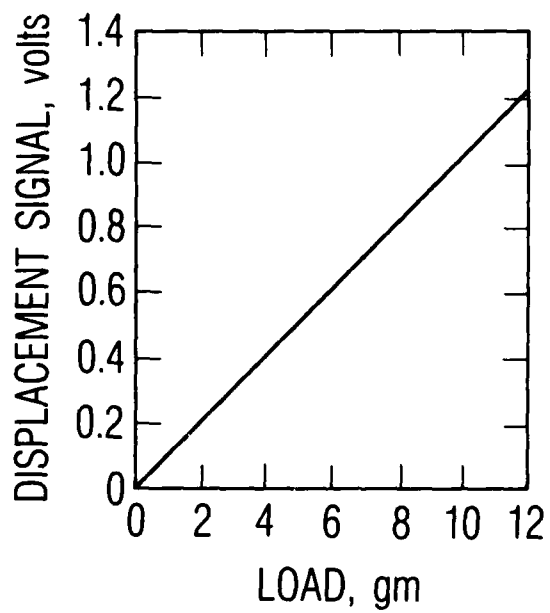
15

Figure 8. Displacement gage force calibration.

A typical test record is shown in Figure 9. In this figure, time increases to the left. The lowest trace is the plenum pressure in psi referenced to the vacuum tank pressure. The oscillating signal is the response of the force model to the side force applied. The upper trace is the pressure in the gas supply tanks. The traces do not appear to start at the same time, but that is because the pens on the recorder are displaced from each other in order to accommodate six channels on the chart. This displacement can be accounted for in the calibration. The side force is determined from an average value of the oscillating signal. The thrust is calculated from the plenum pressure.

When the experiments were begun, we noted an alignment problem in the nozzles then in use. When the nozzle positions were rotated, a side force was measured which was related to the nozzle azimuthal position. We therefore built new nozzles; located the minimum side force position using the straight plenum supply tube, and located the pivot position which produced the minimum side force signal. This position, it was assumed, is the one in which the thrust line goes through the axis of rotation.
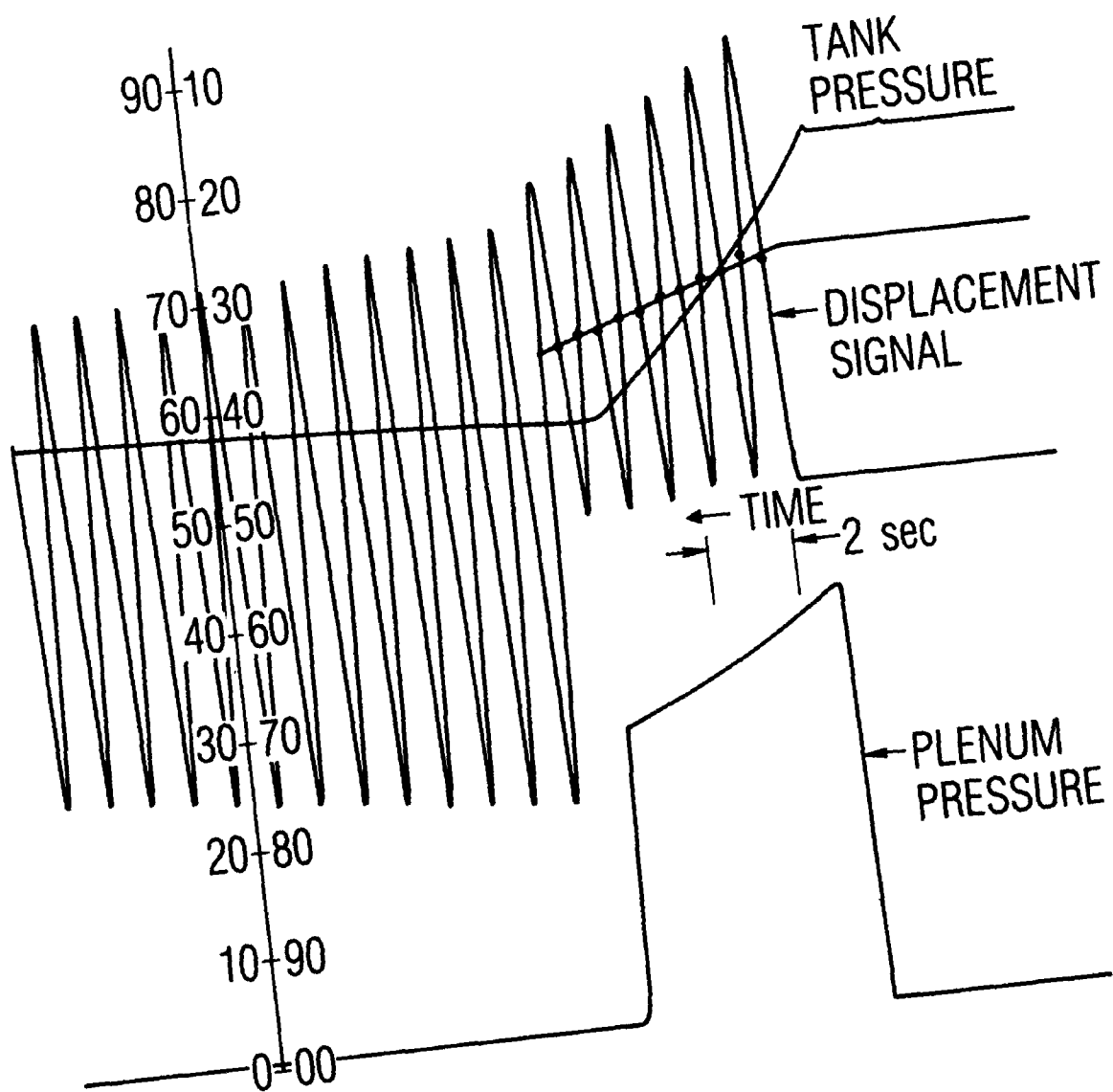
17

Figure 9. Typical force measurement.

18

III. RESULTS AND CONCLUSIONS

The results of these tests are summarized in Figures 10 and 11 for the short nozzle and the longer compensated nozzle. In these figures, the measured side force normalized with respect to the thrust calculated from the measured plenum pressure is plotted as a function of plenum pressure. During a test, the plenum pressure decreases with time as the gas storage tanks are depleted. To reduce the data, we make three measurements of the side force and plenum pressure; at the beginning of the trace, the middle, and at the end. Hence, each test is represented by three points on Figures 10 and 11 for three plenum pressures.

For the short nozzle, the results seem unequivocal. For the nozzle entrance flow inclined in one direction, e.g., bent tube east, there appears to be a side force in that direction. When the entrance flow is rotated 180 deg, i.e., bent tube west, the force is also.

For the long nozzle, the forces are indeed made smaller than for the short nozzle as expected from the analyses in References 2 and 3, which predict that side force varies in a damped sinusoidal manner with nozzle length.

Cone angle and throat radius of curvature for nozzles 3 and 4 are much different from those upon which the analyses were based. Therefore, we built new nozzles (Figure 7), in which the cone half angle α and the throat radius of curvature-to-throat-radius-ratio, $\rho_t/y_t = \lambda$, were the same as those values of one of the nozzles studied by Hoffman and Maykut (Reference 3). Their predictions for this nozzle for $\alpha = 10$ deg and $\lambda = 0.5$ and plenum conditions of 1000 psi, 6000°R, $\gamma = 1.2$ are reproduced in Figure 12. We then measured side force for this nozzle for three nozzle lengths, $x/y_t = 12$, 6, and 3. The side force values obtained are plotted in Figure 12. For these tests, plenum temperature and pressure are 296°K, and 450 psi. The mass flow rate is determined from plenum conditions according to

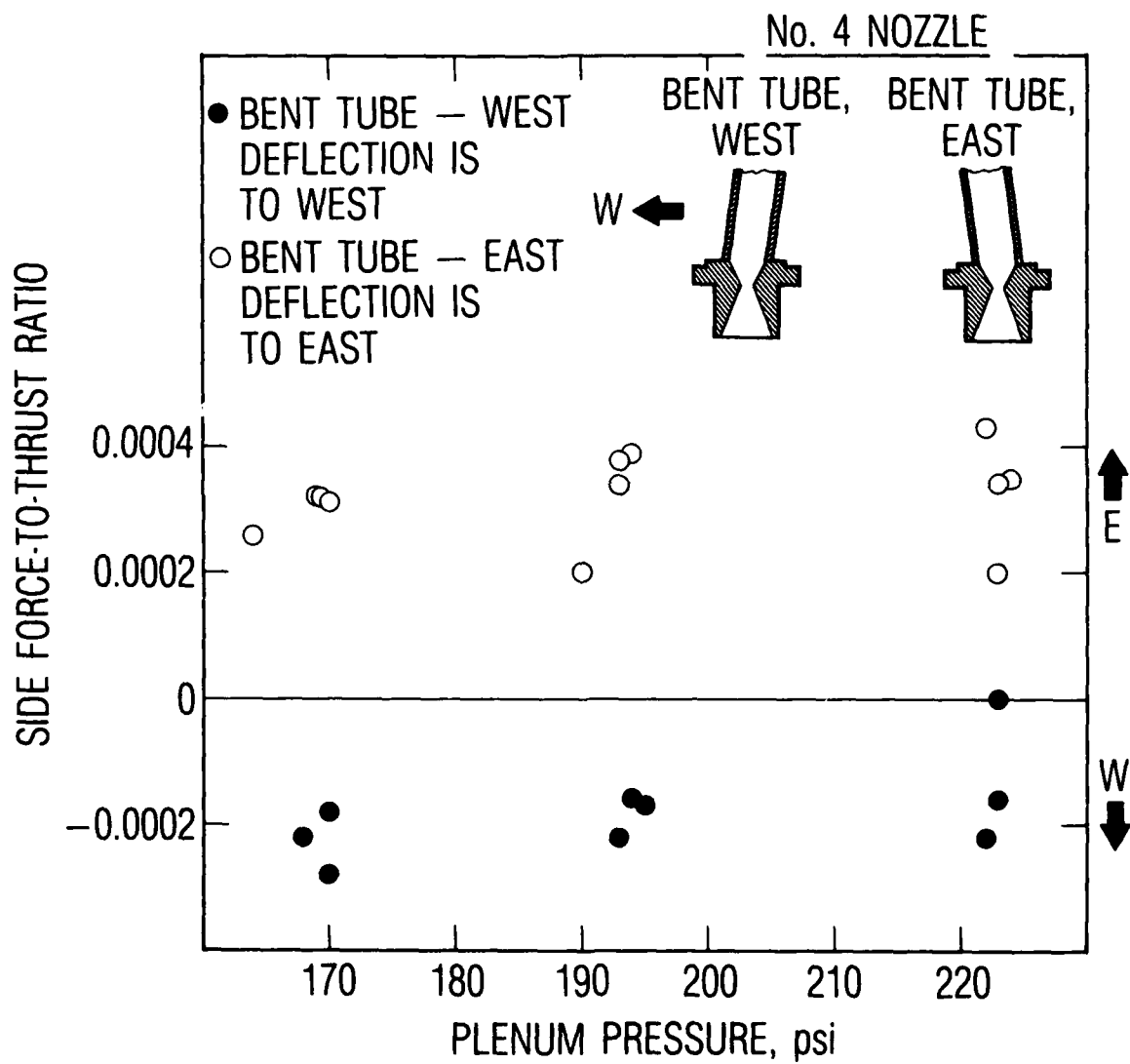$$\dot{m} = 0.579 \sqrt{\frac{\gamma}{RT_o}} \, p_o A^* .$$

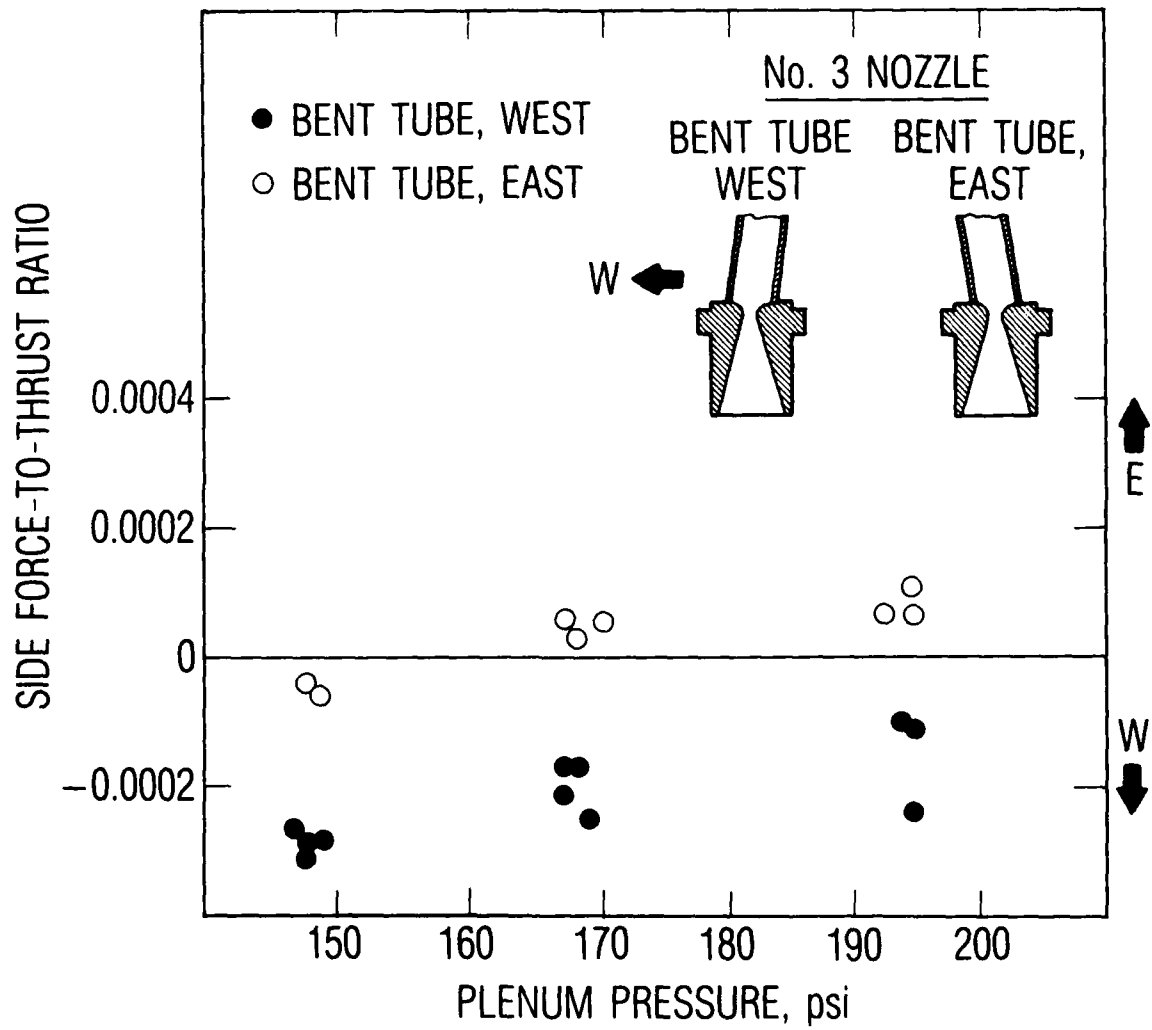Figure 10. Effect of plenum asymmetry on nozzle side force.

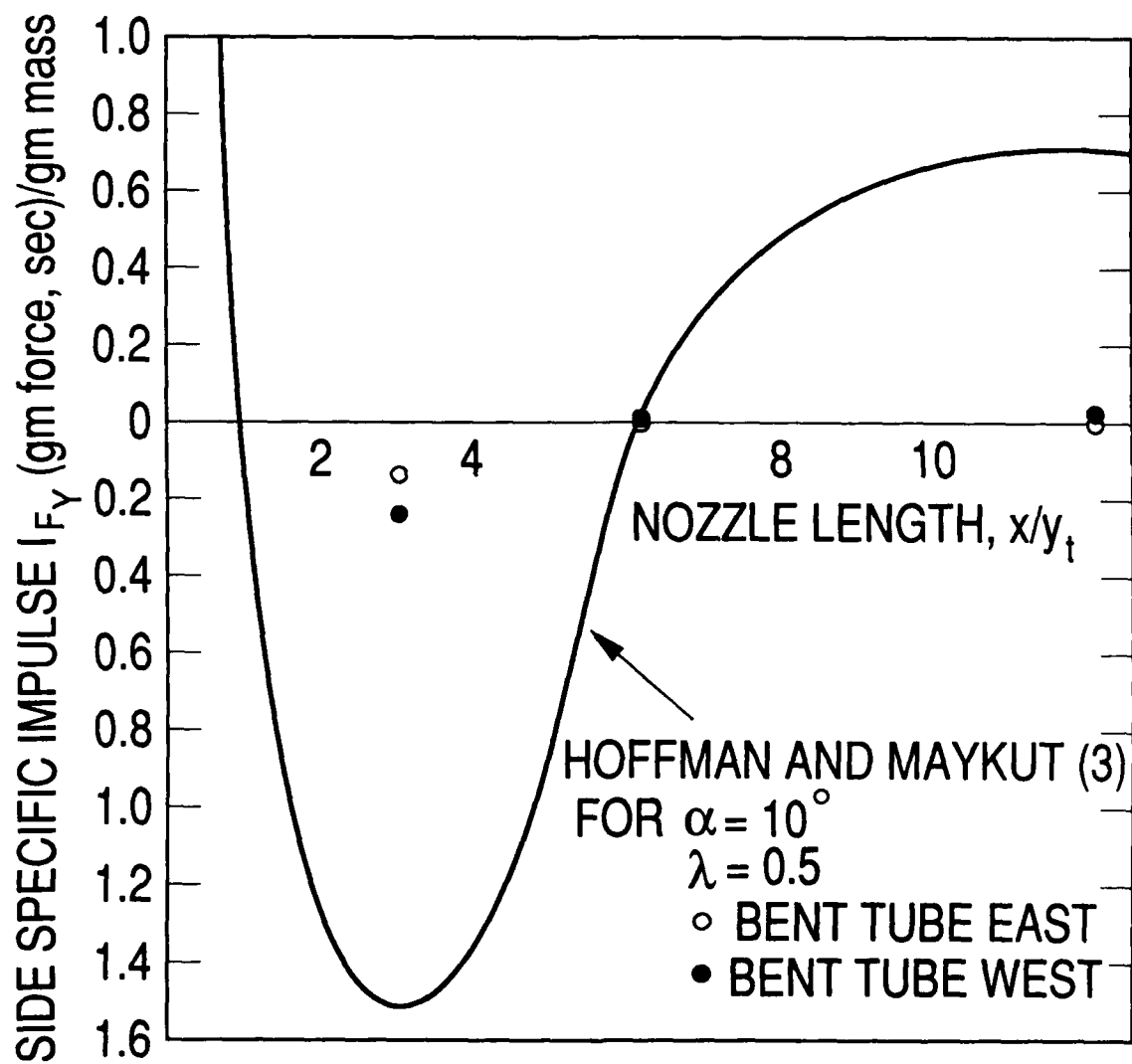Figure 11. Effect of plenum asymmetry on nozzle side force.

Figure 12.   Effect of nozzle length on side force;
comparison with Reference 3.

22

$\gamma = 1.4$ and R is the gas constant for nitrogen. Subscript zero refers to plenum conditions.

These results demonstrate the predicted effect of nozzle length on the measured side force. For $x/y_t = 12$ and for plenum flow angled to the west, the largest positive side force occurs (deflection to the east is positive in our laboratory system). For $x/y_t = 3$, the side force swings to the west, and at $x/y_t = 6$, it is close to zero.

The initial direction of the flow at the throat entrance section for nozzles 5, 6, and 7 appears to have little effect on the direction and magnitude of the side force compared to the effect of the nozzle length. For nozzles 3 and 4, when the tube leading to the nozzle entrance section was inclined to the west, the observed side force was inclined to the west (Figure 10) or at least inclined west of the direction resulting when the tube was inclined to the east (Figure 11).

For nozzles 5, 6, and 7 however, the westward inclining nozzle produced eastward directed side force until the side force went to zero ($x/y_t = 6$). Then it appeared that the force and entrance flow direction again agreed.

The magnitude of the side force is of the order of 10^{-4} of the thrust. This value is very low compared to those values predicted and measured in References 2 to 4 and shown in Figure 12. We could, at this point, conclude that when the flow is inclined in the plenum, some straightening can occur during compression in the converging part of the nozzle. Thus, the asymmetry at the throat may be greatly reduced. Therefore, the observed side forces may be much reduced compared with when the flow is canted at the nozzle throat. But to confirm this viewpoint, we took nozzle 3 and modified it by tilting the throat as shown in Figure 13. We also examined the effect of mass flow by extending the plenum pressure and hence the mass flow rate through the nozzle.

The results of these measurements are shown in Figure 14. The side force generated when the nozzle throat is tilted (that is, when the asymmetry in the flow is extended to the plane of the throat) is much greater than when the

23

asymmetry is limited to the plenum. In fact, the effect of the plenum flow misalignment, as exhibited in Figure 11 by the open and closed circles, is masked by the effect of the asymmetric throat as shown in Figure 14.

It seems reasonable to conclude, therefore, that when the nozzle and throat entrance section are properly axisymmetric, the effect of misalignment of the flow entering the throat is small relative to the effects of misalignment of the throat itself.
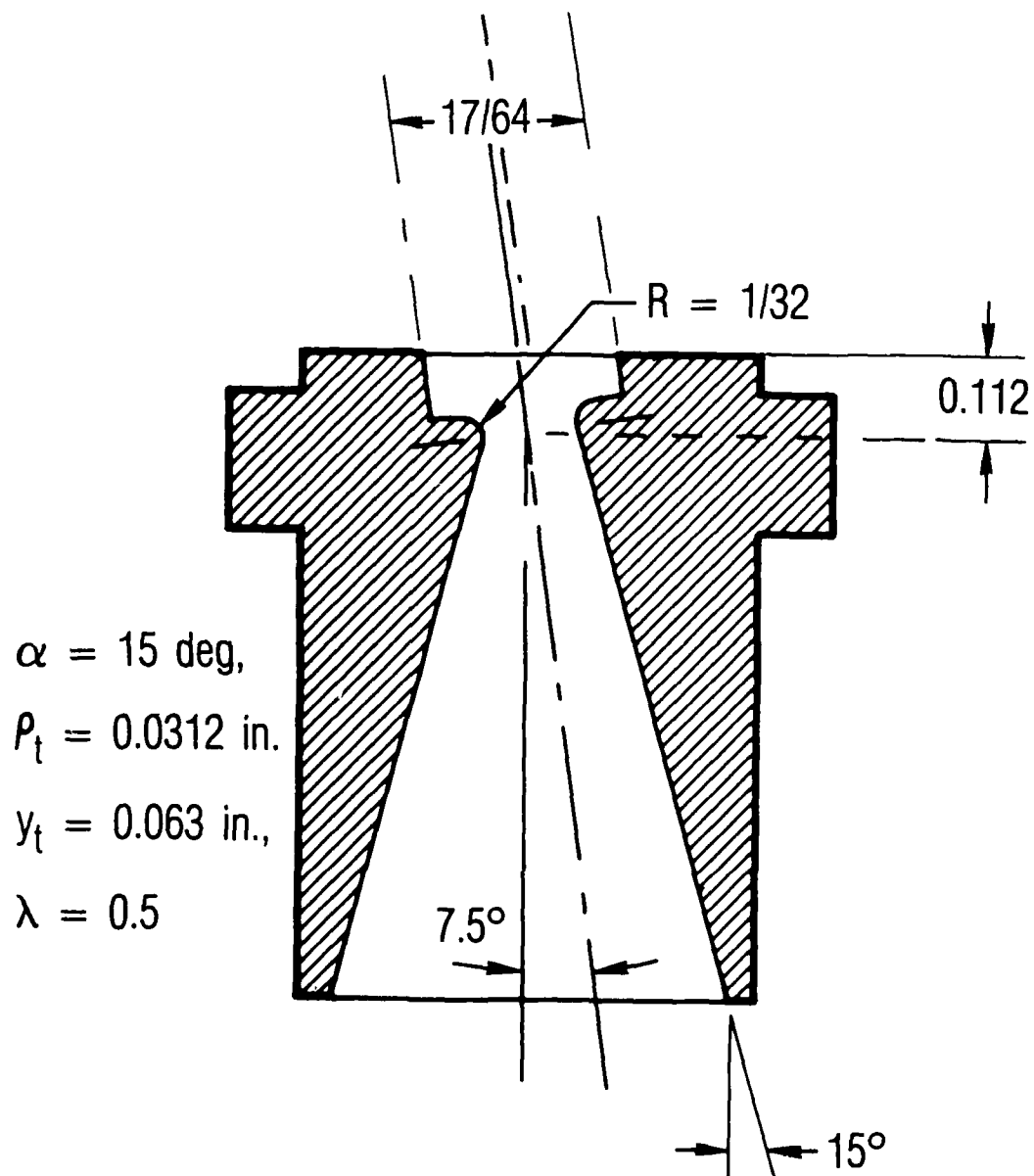
Figure 13. Number 3 nozzle modified for inclined throat flow.
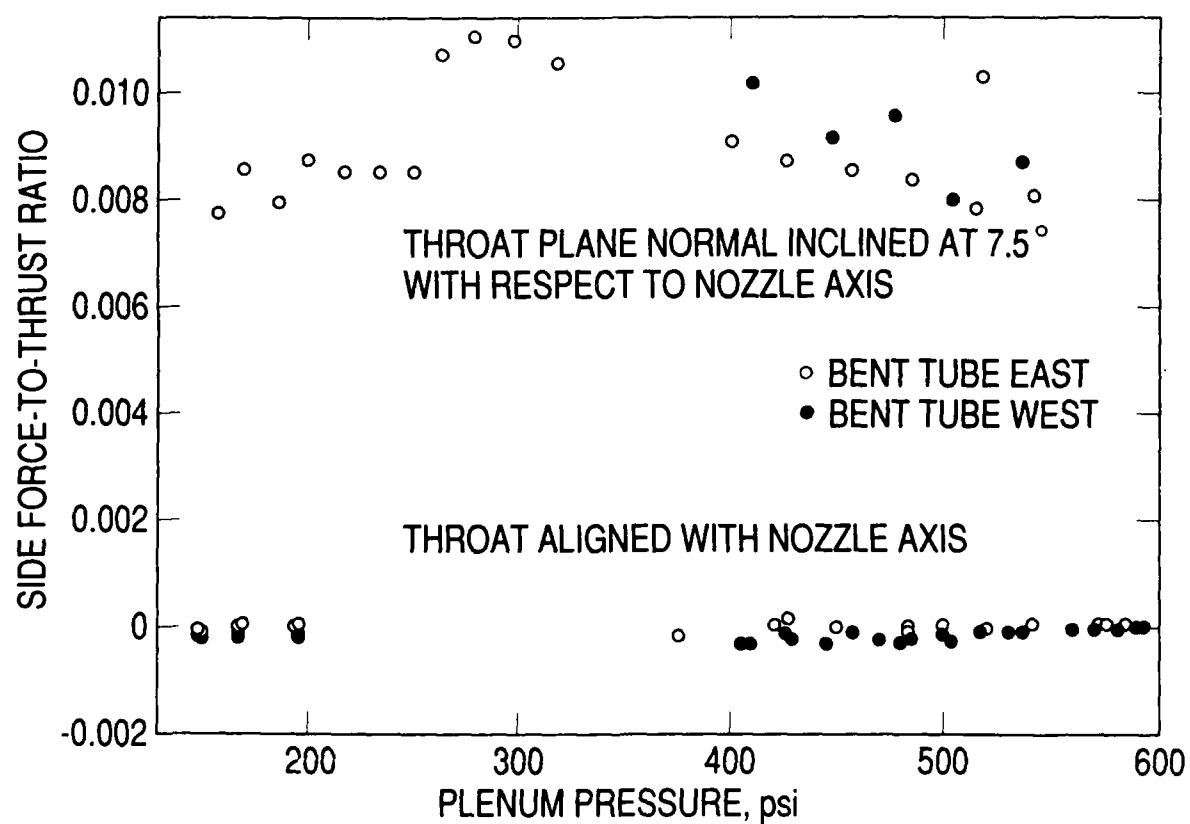
The figure includes the following labels:

17/64

R = 1/32

0.112

α = 15 deg,

P_t = 0.0312 in.

y_t = 0.063 in.,

λ = 0.5

7.5°

15°

Figure 14. Effect of nozzle throat alignment on side force, nozzle number 3.

IV. SUMMARY

The Star 48 upper stage rocket motor and payload system appears to precess in a coning motion which affects the flight path. The coning motion has been attributed to side forces generated because of deviations of the rocket nozzle entrance flow from truly axisymmetric conditions. In this report, an experimental investigation is described in which intentional nozzle entrance flow misalignment was produced and consequent side force was measured on a model at a simulated altitude of 1.7×10^5 ft.

Side forces generated with an approximately 1/50th scale Star 48 rocket nozzle were quite small when compared to the predictions and measurements of previous investigators, but the difference was attributed to the difference where the flow inclination or misalignment occurs. When the flow is inclined at the nozzle throat, the downstream effect of the inclination is predictably large. When the flow is inclined in the plenum upstream of the nozzle entrance, the downstream effect is smaller by an order of magnitude. The observed side forces show a dependence on the nozzle length, as indicated by earlier investigators.

REFERENCES

1. Meyer, R. X., "Internal Flow in a Precessing Solid Propellant Rocket Motor," 29th Heat Transfer and Fluid Mechanics Institute, 1985.

2. Darwell, H. M., Trubridge, G. F.P., "Design of Rocket Nozzles to Reduce Gas Misalignment," J. Spacecraft, 5, 1, January 1968, pp. 36-41.

3. Hoffman, J. D., and Maykut, A. R., "Gas Dynamic Gain of Supersonic Thrust Nozzles," J. Spacecraft, 11, 10, October 1974, pp. 697-704.

4. Walters, A. G., "Non-Symmetric Flow in Laval Type Nozzles," Phil Trans. Royal Soc. London, 273, A 1232, September 1972, pp. 185-235.

LABORATORY OPERATIONS

The Aerospace Corporation functions as an "architect-engineer" for national security projects, specializing in advanced military space systems. Providing research support, the corporation's Laboratory Operations conducts experimental and theoretical investigations that focus on the application of scientific and technical advances to such systems. Vital to the success of these investigations is the technical staff's wide-ranging expertise and its ability to stay current with new developments. This expertise is enhanced by a research program aimed at dealing with the many problems associated with rapidly evolving space systems. Contributing their capabilities to the research effort are these individual laboratories:

Aerophysics Laboratory: Launch vehicle and reentry fluid mechanics, heat transfer and flight dynamics; chemical and electric propulsion, propellant chemistry, chemical dynamics, environmental chemistry, trace detection; spacecraft structural mechanics, contamination, thermal and structural control; high temperature thermomechanics, gas kinetics and radiation; cw and pulsed chemical and excimer laser development including chemical kinetics, spectroscopy, optical resonators, beam control, atmospheric propagation, laser effects and countermeasures.

Chemistry and Physics Laboratory: Atmospheric chemical reactions, atmospheric optics, light scattering, state-specific chemical reactions and radiative signatures of missile plumes, sensor out-of-field-of-view rejection, applied laser spectroscopy, laser chemistry, laser optoelectronics, solar cell physics, battery electrochemistry, space vacuum and radiation effects on materials, lubrication and surface phenomena, thermionic emission, photo-sensitive materials and detectors, atomic frequency standards, and environmental chemistry.

Computer Science Laboratory: Program verification, program translation, performance-sensitive system design, distributed architectures for spaceborne computers, fault-tolerant computer systems, artificial intelligence, micro-electronics applications, communication protocols, and computer security.

Electronics Research Laboratory: Microelectronics, solid-state device physics, compound semiconductors, radiation hardening; electro-optics, quantum electronics, solid-state lasers, optical propagation and communications; microwave semiconductor devices, microwave/millimeter wave measurements, diagnostics and radiometry, microwave/millimeter wave thermionic devices; atomic time and frequency standards; antennas, rf systems, electromagnetic propagation phenomena, space communication systems.

Materials Sciences Laboratory: Development of new materials: metals, alloys, ceramics, polymers and their composites, and new forms of carbon; non-destructive evaluation, component failure analysis and reliability; fracture mechanics and stress corrosion; analysis and evaluation of materials at cryogenic and elevated temperatures as well as in space and enemy-induced environments.

Space Sciences Laboratory: Magnetospheric, auroral and cosmic ray physics, wave-particle interactions, magnetospheric plasma waves; atmospheric and ionospheric physics, density and composition of the upper atmosphere, remote sensing using atmospheric radiation; solar physics, infrared astronomy, infrared signature analysis; effects of solar activity, magnetic storms and nuclear explosions on the earth's atmosphere, ionosphere and magnetosphere; effects of electromagnetic and particulate radiations on space systems; space instrumentation.